Assessing Silt Generation and Origins in Granitoid-Hosted Soils: Implications for Loess Formation

Alicia L. Bonar[1], Gerilyn S. Soreghan[1], and Megan E. Elwood Madden[1]

[1]University of Oklahoma, School of Geosciences, Norman, Oklahoma 73019, U.S.A.

Corresponding author: Alicia Bonar (alicia.bonar@ou.edu)

Key Points:

- Intense chemical weathering associated with soil formation in hot-humid climates generates abundant silt to clay-sized particles from coarse-grained bedrock.
- Pedogenic processes likely do not play a major role in silt generation for loess formation.

Abstract

The origin and production of silt are key factors in the formation of loess deposits. Although many processes can potentially lead to silt generation, few are known to produce silt in the volumes and particle-size modes required to form geologically significant loess deposits. Here we investigate the hypothesis that pedogenic weathering in tropical and Mediterranean climates can generate abundant *in situ* silt, and therefore contribute significantly to loess formation throughout geologic time. We utilize granulometric and geochemical data from soils formed in Puerto Rico (hot-humid) and Southern California (hot-arid) to discern whether the mud fraction (<62.5 μm) is generated from bedrock (autochthonous) or sourced from eolian contributions (allochthonous). Our study demonstrates that the Puerto Rico soil contains abundant (up to 72%) silt- and clay-sized grains compared to the Anza Borrego soil (<6%). However, the silt fraction of the Puerto Rico soil is at least partially derived from eolian inputs, and the silt fraction of the Anza Borrego soil is geochemically indistinguishable from allochthonous dust sources. Furthermore, while intense chemical weathering in a tropical climate can produce abundant fines, the majority are significantly finer (average mode ~15 μm) than the modes of most "typical" loess deposits (modes more than 20 – 30 μm). In contrast, weathering in Mediterranean climates produces volumetrically sparse silt. Hence, pedogenic weathering in hot climates appears to be ineffectual for producing the volume and size distributions of silt-sized material needed to generate significant loess deposits.

Plain Language Summary

Global sediment movement is important to understand when reconstructing Earth's past geography and climate. Windblown silt deposits, known as loess, are particularly useful for recording paleoclimatic conditions, but the origin of the silt that forms large loess accumulations remains controversial. In this study, we aim to better understand processes that can generate silt in large quantities by investigating whether significant silt is formed in place as soils from underlying bedrock or if the silt observed in soils was delivered from elsewhere. We compare silt in two different soils, one from a hot-dry climate and one from a hot-wet climate, which provides additional information about how weathering processes can influence the results. Our findings demonstrate that soil forming in the hot-wet climate can create abundant silt, but with a grain size smaller than most loess deposits, whereas soil from hot-dry climates produces minimal silt. Additionally, both soils show evidence for silt inputs from local and regional dust sources. Our results suggest that soil formation is not a major process for silt production that contributes to loess deposits.

1 Introduction

Loess is a significant component of the terrestrial rock record in the Quaternary (e.g., Catt, 1988; Smalley, 1995; Assallay et al., 1998; Muhs and Bettis, 2003; Muhs, 2013; Li et al., 2020) and covers approximately 6% of Earth's surface today (Li et al., 2020). The largest deposits are spatially linked to former ice margins and typically found in mid – high latitude regions (Catt, 1988; Smalley, 1995). Hence, glacial grinding is known to be an especially efficacious way to generate large quantities of silt (Pye, 1995; Smalley, 1995; Assallay et al., 1998; Soreghan et al., 2008) in typical loess grain size modes (~20 – 40 μm; e.g., Smalley and

Krinsley, 1978; Tsoar and Pye, 1987; Assallay et al., 1998; Anderson, 2007). However, smaller accumulations of loess and loess-like deposits also occur in lower-latitude hot climates— for example, the Negev loess in Israel— indicating that silt that forms loess deposits can be produced by processes unrelated to glaciation (e.g., Pye and Tsoar, 1987; Crouvi et al., 2008). Therefore, eolian saltation and abrasion in desert environments have also been suggested as processes for silt generation (Smalley and Vita-Finzi, 1968; Tsoar and Pye, 1987; Smith et al., 2002; Crouvi et al., 2008; Enzel et al., 2010), although experiments using realistic wind velocities and starting material indicate that saltation abrasion produces insufficient silt to form loess (e.g., Kuenen, 1960; Swet et al., 2019; Adams and Soreghan, 2020). Furthermore, fluvial comminution (Wright and Smith, 1993), as well as insolation-, salt-, and frost-weathering (e.g., Pye and Sperling, 1983; Wright et al., 1998; Wright, 2001) have also been suggested to generate silt, but no systematic data exist that illustrate the efficacy of producing large volumes of silt by these means.

Pedogenic weathering has also been widely suggested as a potential means for silt production in warm climates (e.g., equatorial, tropical, and Mediterranean) originally by Nahon and Trompette (1982), and subsequently reiterated by others (e.g., Wright, 2001, 2007). Nahon and Trompette (1982) argued that chemical weathering in soils can form abundant silt-sized quartz and feldspar grains and predicted that mature soil profiles that develop on even coarse-grained, granitoid bedrock can contain between 50 – 75% silt-sized grains. They suggested that the primary mechanism for creating this silt is the breakdown of crystals in intense combinations of chemical and physical weathering, resulting in fragmentation due to dissolution along subplanar microfractures now known as Moss defects (Moss, 1966; Moss and Green, 1975). Wright (2007) supported this claim that pedogenic weathering can be a key contributor to silt production through their review of the efficacy of weathering processes to generate fine-grained material on a variety of parent rocks, as well as analysis of grain-size characteristics in weathering profiles.

Nahon and Trompette (1982) based their hypothesis on examination of thin sections illustrating the presence of many fine grains (both quartz and feldspar) with uniform extinction that appear to have been components of a pre-existing single crystal, indicating the *in situ* breakdown of larger crystals. They also cited an increasing abundance of silt- and clay-sized quartz grains at the tops of weathering profiles, which they attributed to the progressive dissolution of quartz from the bedrock up-profile (Nahon and Trompette, 1982; Wright, 2001). Additionally, mature weathering profiles can be greater than 10 meters in thickness, especially in humid climates, and tropical, equatorial, and Mediterranean soils typically contain ferruginous or carbonate matrices, which can readily disaggregate to ultimately release the entrained silt. However, the efficacy of pedogenic weathering for silt production has not been tested rigorously – experimentally or empirically.

Here, we test the hypothesis of abundant pedogenic generation of silt in warm-climate soils by assessing the grain size and geochemistry of silt recovered in a hot-wet (tropical) weathering profile from southeastern Puerto Rico and a hot-dry (Mediterranean) profile from the Anza Borrego Desert, southwestern United States (U.S.). Our results highlight significant differences in the potential for *in situ* silt generation in soils from these varying climates, both in terms of the volume and particle size modes of produced silt. These results contribute to our understanding of the formation of loess deposits through Earth history, and their possible paleoclimatic significance.

2 Geologic Setting

We focused on two localities, each characterized by granitoid bedrock and hot climates, but contrasting precipitation: arid-hot Anza Borrego Desert in southern California (southwestern U.S.) and wet-tropical southeastern Puerto Rico (Caribbean Islands; Fig. 1). Refer to Table 1 for details regarding climate classification and soil formation variables including bedrock geology and dust influences. Both study regions are hosted primarily on crystalline granitoid bedrock characterized by a relatively coarse grain-size (Fig. 2, 3). In addition to potential *in situ* formation of silt in the soil profiles, both locations receive either local dust or long range traveled (LRT) dust (Table 1; references within). We sampled surficial profiles characterized as "modern," that likely record time-averaged dynamic climatic conditions of the late Pleistocene. For example, southern California experienced a wetter climate during interglacials of the Quaternary (e.g., Reheis et al., 2012), and Puerto Rico was influenced by glacial and interglacial cycles through changing sea levels which likely affected vegetation and biodiversity (e.g., Weigelt et al., 2016).

In southern California, the study area encompasses Indian Gorge within the southern part of the Anza Borrego Desert (Fig. 1A), where the bedrock geology consists of the Middle Cretaceous La-Posta tonalite (Fig. 2) overlain by first-cycle Quaternary alluvial sediment (of late Pleistocene or younger age; Fletcher et al., 2011; Blisniuk et al., 2012). Both the bedrock and derived alluvial sediment contain majority plagioclase, quartz, biotite, and potassium feldspar (Clinkenbeard and Walawender, 1989; Joo et al., 2016). Allochthonous eolian material is likely delivered to the Anza Borrego Desert by seasonal Santa Ana wind events from the Greater Mojave Desert region (Muhs, 1983; Reheis et al., 1995, 2002; Muhs et al., 2007a; Fig. 1A). Previous studies document the grain size distribution of Mojave Desert dust as mostly silt (up to 70%) with some clay-sized material (20 – 45%; Reheis et al., 1995)

The Puerto Rico study area lies within the Rio Guayanés watershed of southeastern Puerto Rico (Fig. 1B). The Rio Guayanés watershed is underlain predominantly by the Late Cretaceous San Lorenzo granodiorite, as well as first-cycle alluvium (Rogers et al., 1977), both of which contain plagioclase, quartz, potassium feldspar, hornblende, and chlorite with minor accessory minerals (Fig. 2; Joo et al., 2018). Dust deposition on the Caribbean Islands is well established from previous studies (Table 1), with two major sources identified: Saharan and Sahel desert dust from North Africa and volcanic ash from the Lesser Antilles volcanic arc in the eastern Caribbean Sea. More than 60 million tons of Saharan dust is deposited annually (Prospero and Lamb, 2003; Lau and Kim, 2007). African dust from the Saharan and Sahel deserts contains mostly fine-silt sized quartz (4 – 20 μm) and clay-sized (<4 μm) mica; 30 – 50% of the dust is <2.5 μm (e.g., Prospero et al.,1970; Glaccum and Prospero, 1980). Volcanoes within the Lesser Antilles have been active since the Pleistocene (e.g., Frey et al., 2018), with multiple explosive eruptions recorded in marine sediments west of the arc (e.g., Carey and Sigurdsson, 1978; Sigurdsson and Carey, 1980; Le Friant et al., 2008). Many of the tephra units contain plagioclase, augite, hornblende, rhyolite glass, and some quartz, with the largest phenocrysts ranging in size from 0.5 – 2 mm (e.g., Carey and Sigurdsson, 1980). There is also considerable silt-sized crystals and glass within the ashfalls, with glass content increasing with decreasing grain size (Carey and Sigurdsson, 1980).

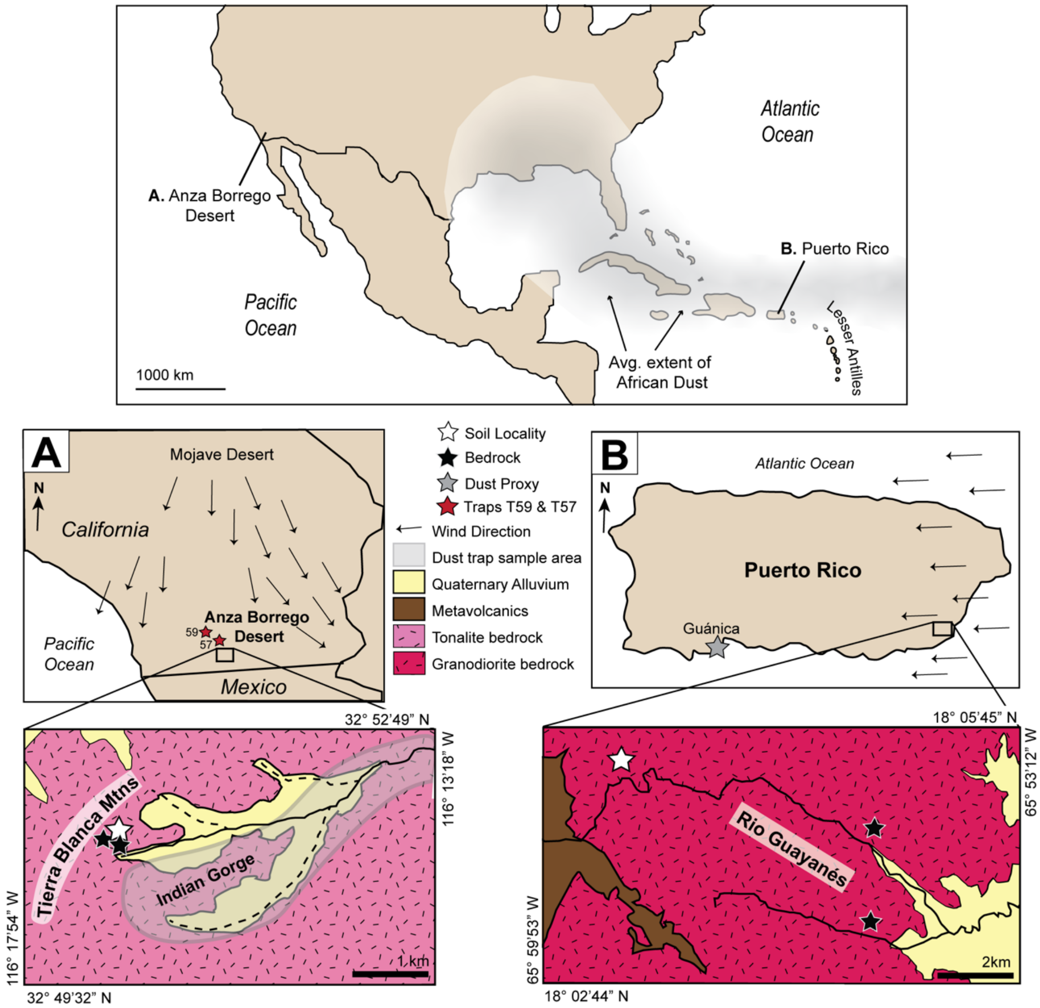

Figure 1. Regional geographic map showing both study localities within southern North America, the average extent of African dust during summer, and the location of the Lesser Antilles volcanic arc. Zoomed-in study areas are shown in A and B with representative wind directions, soil (white star), bedrock (black star), and dust trap (red star)/proxy (grey star) locations. A) Anza Borrego Desert in Southern California and relative directions for Santa Ana wind events from the north/northeast (modified from Muhs et al., 2007b). Locations for dust traps T57 and T59 are outside the zoomed-in study area (from Reheis and Kihl, 1995). The Indian Gorge ephemeral-stream system (black and black dashed lines) is covered in Quaternary alluvium while the surrounding area and Tierra Blanca Mountains expose Cretaceous tonalite bedrock. Dust trap sample area is highlighted in light gray (modified from Joo et al., 2016). B) Rio Guayanés watershed (black lines) in southeastern Puerto Rico and relative direction of Lesser Antilles Arc and African dust movement from the east, and location of the dust proxy (gray star) in southern Puerto Rico. The eastern extent of the watershed is covered by Quaternary alluvium and the majority of the study area is exposed granodiorite bedrock (modified from Joo et al., 2018).

Field Locality Variable	Anza Borrego Desert	Southeastern Puerto Rico
Climate Classification [1]	Csa - hot-dry summer Meditteranean	Af - tropical rainforest
Mean Annual Temperature [2, 3]	23˚C	27˚C
Mean Annual Precipitation [2, 3]	132 mm	1382 mm
Bedrock type [4]	tonalite and first-cycle alluvial sediment	granodiorite
Potential dust influence [5]	Greater Mojave Desert, local Anza Borrego Desert	Africa (Saharan and Sahel Deserts), Lesser Antillies volcanism

[1] *Beck et al. (2020)*
[2] *NOAA Climate Normals, 1991-2020, Station Borrego Desert Park*
[3] *NOAA Climate Normals, 1991-2020, Station Guayama 2E*
[4] *Rogers et al. (1977); Clinkenbeard and Walawender (1989); Joo et al. (2016, 2018)*
[5] *Muhs (1983); Muhs et al. (2007a, 2007b); Reheis et al. (1995, 2002)*

Table 1. Summary of climate classifications and soil formation variables for the Anza Borrego Desert and southeastern Puerto Rico field localities.

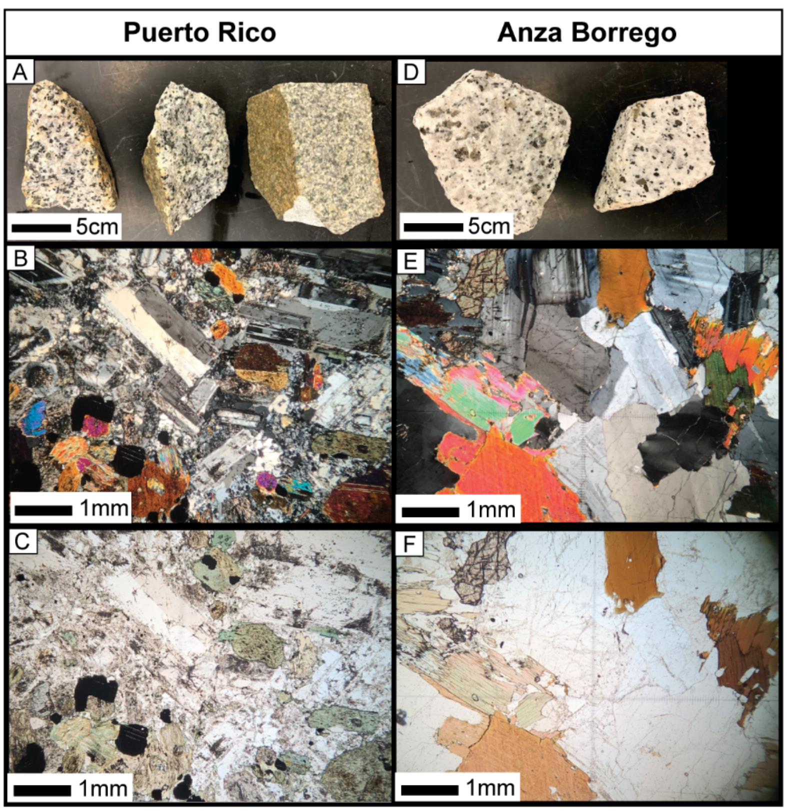

Figure 2. Hand sample photographs (A, D) and thin section photomicrographs (B, C, E, F). for the Anza Borrego and Puerto Rico bedrock samples. B) representative photomicrograph depicting typical crystal size, weathering, and mineralogy of the San Lorenzo granodiorite from Puerto Rico (XPL); C) photomicrograph from B in PPL E); representative photomicrograph

depicting typical crystal size, weathering, and mineralogy of the La-Posta tonalite from Anza Borrego (XPL); F) photomicrograph from E in PPL.

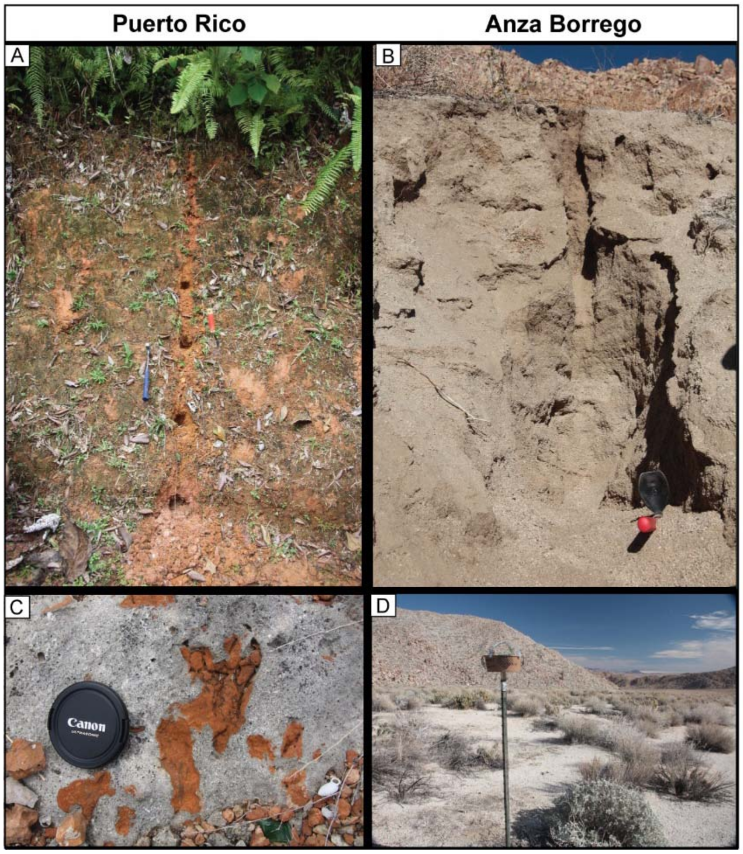

Figure 3. Field photos of soil profiles and dust samples for each study locality. A) Puerto Rico soil and sub-sample locations; hammer for scale. B) Anza Borrego soil; minimal soil integrity prevented sub-sample location preservation; trowel for scale. C) Pleistocene beach rock from the shoreline in Guánica used as a dust proxy for Puerto Rico. The orange, dust-derived sediment filled in karst-openings in the carbonate; camera lens-cap for scale. D) Example of dust trap apparatus (~ 1.75 m tall) deployed in the Anza Borrego Desert.

3 Methods

3.1 Sample collection

Soil, bedrock, and dust samples were collected from the Anza Borrego Desert in southern California in December 2013. Soil, bedrock, and Pleistocene carbonate beach rock (a proxy dust trap) samples were collected from the Rio Guayanés watershed in southeastern Puerto Rico in 2014 (Fig. 1, 2, 3). Anza Borrego soil samples (N=7, ~20 cm spacing) were collected along the Indian Gorge in the Tierra Blanca Mountains from a 1.5-m profile formed on first-cycle proximal alluvial fan sediment atop tonalite bedrock (N=3). Dust traps (a total of 12, patterned after designs in Reheis and Kihl,1995 and Reheis, 2003; Fig. 2A) were deployed throughout the area, but only one trap was salvageable (N=1). Due to the low volume of dust collected, we obtained two dust trap samples from Marith Reheis (dust traps T57 and T59; Reheis and Kihl, 1995) to supplement our dataset. Puerto Rico soil samples (N=6, ~50 cm intervals) were collected from a 2.5-m profile formed on granodiorite bedrock (N=2). Dust traps were deployed in the Puerto Rico study area (total of 5, using the same model as the Anza Borrego locality) but did not survive the deployment. Instead, we collected samples of Pleistocene carbonates with karst-filling mudstones from the southern coast near Guánica as a proxy dust sample (N=1; Fig. 1B).

3.2 Sample pre-treatment and analysis

Representative subsamples of the soil profile were first wet-sieved to assess proportions of gravel (> 2 mm), sand (63 μm – 2 mm), and mud (< 63 μm). A subsample of the muds from all samples were treated with buffered acetic acid for 24 hours to remove carbonates and 30% hydrogen peroxide (up to 2 weeks) to remove organic matter. Owing to the high carbonate content of the Pleistocene beach rock, this sample was processed with 2N HCl for 24 hours to fully disaggregate the sample prior to hydrogen peroxide treatment. Processed subsamples were used for laser particle size analysis (LPSA) and whole rock, trace element, rare earth element, and base metal geochemical analyses. Samples analyzed by the LPSA were run in triplicate to ensure reproducibility of histograms and reported modes. The small volume recovered from our Anza Borrego trap precluded LPSA analysis, as all material was used for geochemical analysis; however, dust traps T57 and T59 (Reheis and Kihl, 1995) were used for LPSA. We further wet sieved the Puerto Rico mud samples to compare the chemistry of the < 20 μm mud fraction, the 20 – 63 μm fraction, and the total < 63 μm fraction. We note that all 3 fractions produced comparable geochemical compositions (refer to supplemental data); therefore, we elected to only present data from the total < 63 μm fraction for direct comparison with the other sediment samples.

We used the Wentworth Scale size classification customarily used by sedimentologists (Wentworth, 1922) to describe grain sizes since we apply our interpretations to the deep-time rock record; accordingly, we consider the < 4 μm fraction as clay, and the 4 – 63 μm fraction as silt. LPSA was completed at the University of Oklahoma using a Malvern Mastersizer 3000, where soil and dust samples were combined with distilled water and a few drops of dispersant (sodium hexametaphosphate) and sonicated for 1 minute prior to addition to the LPSA. Crystal size determinations for the bedrock samples were completed by tracing > 100 random crystals from thin sections of each sample and importing the traces into the ImageJ software using the particle size analysis function. Data were reported in area (μm^2), which was used to calculate the 2D diameter (μm) then converted to a 3D measurement using methods described in Johnson (1994). Geochemical analyses were completed by ALS Global using ICP-AES for whole rock analyses; fuse bead, acid digestion and ICP-MS for trace element and rare earth element analysis; and separate four acid digestion for base metal analysis.

4 Results

4.1 Granulometric Data

4.1.1 Anza Borrego

The Anza Borrego soil profile is predominantly gravel (18.2 – 33.1%) and sand (62.1 – 78.8%) with minor (1.2 – 5.6%) mud (Fig. 4; Table 2). Overall, the mud fraction and gravel fractions both increase toward the top of the profile, with the top 0.5 m containing 4.7 – 5.6% mud and 27.5 – 33.1% gravel. The mud fractions exhibit coarse-silt modes of 36 – 42 µm (average ~40 µm) that are invariant throughout the profile, with fine-skewed, relatively unimodal distributions (Fig. 4). The mud fraction is predominantly coarse silt (32.8 – 38.2%) with lesser amounts of medium (25.3 – 30.1%) and fine silt (14.9 – 18.4%), and minor very-fine silt (6.9 – 8.6%) and clay (6.2 – 8.3% ; Table 2). The average silt content in bulk samples from the Anza Borrego profile is <5% with only a trace volume of clay-sized material (<0.5%). Dust samples from T57 and T59 report different modes, but similar silt-fraction distributions (Table 2). Dust trap T57 yielded a mode of 83.3 µm (very fine sand), and T59 yielded a mode of 32.1 µm (coarse silt; Table 2, Fig. 4). Note, however, that T57 contains abundant biotite, which produces unreliable laser diffractometry results owing to the platy cleavage.

4.1.2 Puerto Rico

Grain size data in the Puerto Rico soil contrast significantly with those observed in the Anza Borrego samples, containing minor gravel (0 – 1.5%), with significant sand (28.4 – 55.9%) and mud (42.6 – 71.6%; Fig. 4, Table 2). Unlike Anza Borrego, where the average grain size within the mud fraction remains consistent at each depth, the mud fraction of the Puerto Rico soil samples exhibit modes between 6 – 18 µm that decrease towards the surface of the profile. LPSA histograms from the Puerto Rico soil profile exhibit relatively unimodal peaks in the deeper profile, but display finer, bimodal peaks in the uppermost samples (Fig. 4). At 0.1 m, 0.5 m, and 1 m depths, the Puerto Rico soil samples show distinct modes at both ~5 µm and ~18 µm (Fig. 4). The dust proxy sample (siliciclastic fraction of the carbonate rock) is dominated by clay-sized particles (> 60%), with 14% very fine silt, 13.7% fine silt, and approximately 11% coarse and medium-silt combined (Table 2). Histograms of the Puerto Rico dust proxy exhibit bimodal peaks at < 1 µm and ~5 µm, with an average reported mode of 4.9 µm (Fig. 4).

Among the Puerto Rico soil samples and dust proxy (beach rock), the soil samples exhibit the highest fraction of fine silt (25.0 – 29.2%) and clay (21.3 – 31.2%; Table 2) and the dust proxy contains the highest percentage of clay-sized particles (60.9%; Table 2). The soil

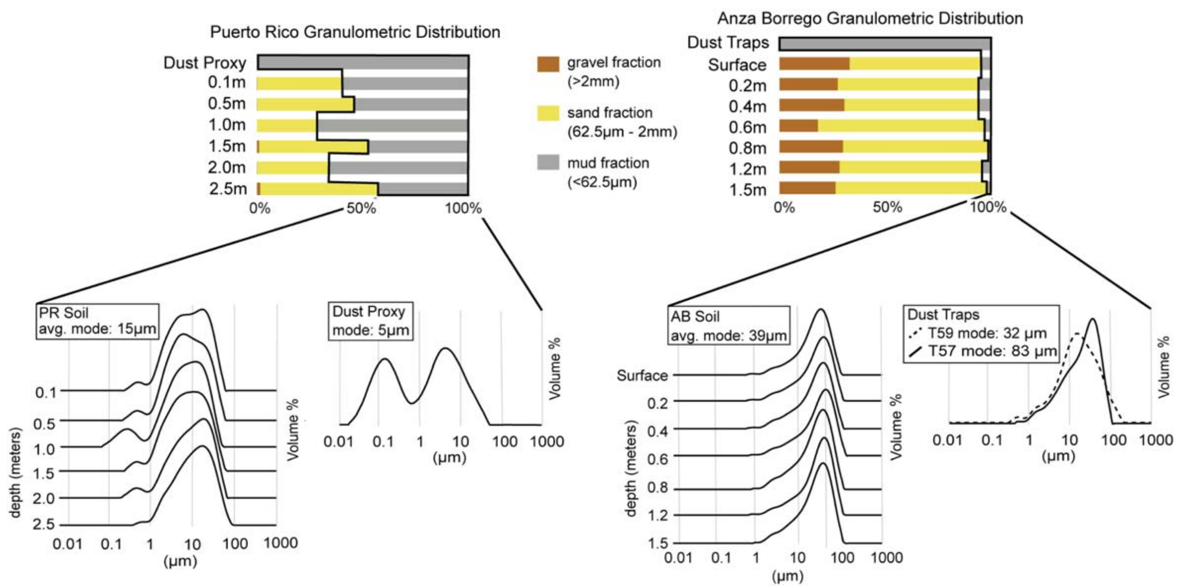

samples contain only minor amounts of coarse silt (4.6 – 8.6%) and moderate medium silt (16.7 – 21.6%). The soil samples exhibit a silt distribution similar to that of the modern dust analog, but have significantly less clay-sized particles (up to 40%). When compared to total soil contents (gravel, sand, and mud fractions), the silt fraction of the Puerto Rico soil ranges from 31 – 50% (Table 2).

Figure 4. Puerto Rico and Anza Borrego soil and dust granulometric distributions. Gravel (brown), sand (yellow), and mud (gray) fractions are represented as bar graphs for each respective soil profile depth out of 100% total soil sample weight. LPSA histograms and average reported modes of the mud fraction are shown for soil and dust samples.

Locality	Sample Descriptions and Depths	Gravel %	Sand %	Mud %	LPSA Results (%): C Silt	M Silt	F Silt	VF Silt	Clay	Avg. Mode (µm)	Mud distribution in total soil (%): C Silt	M Silt	F Silt	VF Silt	Clay	Total Silt %
Anza Borrego	**Dust Trap T57**				26.5	15.2	11.3	7.9	5.8	83.3						
	Dust Trap T59				22.9	20.3	14.1	8.7	7.9	32.1						
	Surface	33.1	62.1	4.7	32.8	30.1	18.4	7.5	7.0	35.5	1.5	1.4	0.9	0.4	0.3	**4.1**
	0.2 m	27.5	66.9	5.5	33.6	28.1	17.5	8.1	7.8	39.2	1.9	1.6	1.0	0.4	0.4	**4.8**
	0.4 m	30.7	63.7	5.6	33.0	27.4	17.6	8.6	8.3	37.7	1.9	1.5	1.0	0.5	0.5	**4.9**
	0.6 m	18.2	78.8	3.0	37.4	25.3	15.0	7.3	6.6	42.3	1.1	0.8	0.4	0.2	0.2	**2.5**
	0.8 m	30.0	68.6	1.4	32.2	27.9	18.4	8.6	7.9	36.6	0.5	0.4	0.3	0.1	0.1	**1.2**
	1.2 m	26.5	69.6	3.9	38.2	27.2	14.9	6.9	6.2	41.1	1.5	1.1	0.6	0.3	0.2	**3.4**
	1.5 m	28.4	70.4	1.2	33.8	27.1	17.6	8.3	7.1	39.5	0.4	0.3	0.2	0.1	0.1	**1.0**
Puerto Rico	**Dust Proxy**				3.6	7.5	13.7	14	60.9	4.98						
	0.1 m	0.2	40.0	59.9	5.9	19.4	26.1	20.8	27.8	17.5	3.5	11.6	15.6	12.5	16.6	**43.2**
	0.5 m	0.0	45.8	54.1	4.6	16.7	25.0	22.4	31.2	6.3	2.5	9.0	13.5	12.1	16.9	**37.2**
	1 m	0.0	28.4	71.6	5.7	18.1	25.7	19.6	30.9	13.9	4.1	13.0	18.4	14.0	22.1	**49.5**
	1.5 m	1.0	51.6	47.4	7.6	18.6	26.1	20.5	27.2	14.1	3.6	8.8	12.4	9.7	12.9	**34.5**
	2 m	0.0	34.1	65.9	6.2	21.1	27.8	19.5	25.4	18.1	4.1	13.9	18.3	12.8	16.7	**49.1**
	2.5 m	1.5	55.8	42.6	8.6	21.6	29.2	19.4	21.3	18.3	3.7	9.2	12.5	8.3	9.1	**33.6**

Table 2. Summary of granulometric analytical results and total silt content percentages for Anza Borrego and Puerto Rico localities. Abbreviations: Coarse (C), medium (M), fine (F), very-fine (VF). Dust samples were not analyzed for gravel, sand, mud distributions.

4.1.3 Bedrock Crystals

Crystal sizes from the Anza Borrego (n=137) and Puerto Rico bedrock (n=204) range from fine to very-coarse crystals (Table 3). Data are reported for calculated crystal area (µm^2), 2D diameter (µm), and converted 3D diameter (µm; Table 3). The diameters are calculated based on the simplification of a spherical shape, and the converted 3D measurements are thus larger than the 2D diameters. Accordingly, these data are a semi-quantitative estimate of bedrock crystal size, but nevertheless demonstrate that both granitoids are coarse-grained; however, the Anza Borrego bedrock crystals are, on average, 2-times larger than the Puerto Rico bedrock (Table 3). The average crystal diameter in the Anza Borrego tonalite is 982 µm, while the average crystal diameter in the Puerto Rico granodiorite is 653 µm (Table 3).

	Area (µm^2 x10^3)		**Diameter (µm)***			
			2D		3D Corrected**	
	AB	**PR**	**AB**	**PR**	**AB**	**PR**
Min	18	18	152	151	158	156
Max	19,020	12,177	4,921	3,938	5,095	4,077
Mean	1,044	459	949	630	982	653
Median	480	224	782	534	809	553

*Diameters are calculated with the assumption of spherical crystals
**Conversion from Johnson (1994)

Table 3. Calculated bedrock crystal sizes from the San Lorenzo granodiorite in Puerto Rico (PR) and the La Posta tonalite in Anza Borrego (AB).

4.2 Geochemical Data

4.2.1 Major Element Geochemistry

Major element geochemistry from the soils, bedrock, and dust samples reflects weathering intensity at the Anza Borrego and Puerto Rico localities (refer to supplementary files for raw data). Major element concentrations were plotted in A-CN-K space using the molar ratios of Al_2O_3-CaO+Na_2O-K_2O following Nesbitt and Young (1984, 1989) to assess weathering trends (Fig. 5). Since all samples were processed to remove carbonate, compositional values of CaO are interpreted to represent values of the silicate fractions. However, after geochemical analysis, an elevated LOI value for the Pleistocene beach rock indicated remnant carbonate bound CaO. The CaO value used for CIA analysis for the Puerto Rico dust proxy is corrected following methods of Taylor and McClennan (1985). CIA values were calculated to understand weathering intensity between each soil compared to potential sources (bedrock and dust) with the following equation using molecular values (Nesbitt and Young, 1982): $[Al_2O_3/(Al_2O_3 + CaO + Na_2O + K_2O)] \times 100$. We note that these values are used only to understand weathering intensity of each soil compared to bedrock, not as a comparison of weathering between each location. As traditionally interpreted, CIA values of 50 – 65 indicate minimal chemical weathering, values of 65 – 85 reflect intermediate chemical weathering, and values >85 indicate extreme chemical weathering (e.g., Nesbitt and Young, 1982, 1984, 1989); however, these values are also affected by the composition of the source material.

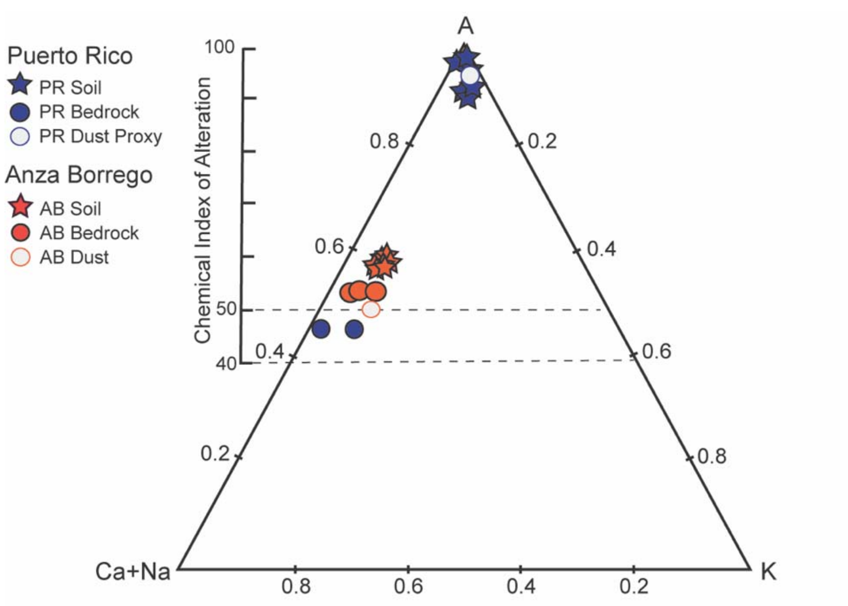

Figure 5. Ternary plot of Puerto Rico (PR) and Anza Borrego (AB) soil, bedrock, and dust sample geochemistry in A-CN-K space with Chemical Index of Alteration (CIA) values labeled on the left. See supplemental files for data references.

In general, the soil samples from Anza Borrego are slightly more Al-rich than the associated bedrock but plot close to bedrock on the A-CN-K ternary diagram. Anza Borrego bedrock samples have CIA values around 50 and the soil samples exhibit CIA values between ~54 – 56, consistent with incipient leaching through chemical weathering relative to the host bedrock. The Anza Borrego dust trap material exhibits the lowest CIA value at 48, indicating that the dust delivered to the Anza Borrego desert was likely derived from more mafic sources.

All Puerto Rico samples plot closer to the CN apex compared to the K apex, attributable to a high fraction of plagioclase in the bedrock (e.g., Joo et al., 2018). Puerto Rico soils are significantly shifted towards the A apex from the host bedrock in A-CN-K space (Fig. 5). Puerto Rico bedrock samples also plot within a similar region as both the Anza Borrego bedrock and soil samples. This indicates that the Puerto Rico soils have experienced significant Ca, Na, and K leaching via chemical weathering. The Puerto Rico bedrock samples exhibit CIA values around 45, consistent with both the Ca-rich bedrock chemistry and minimal chemical weathering of the granitoid bedrock. Puerto Rico soil samples exhibit CIA values of ~85 – 98 indicating uniformly intense chemical weathering compared to the very low values in the bedrock. The Puerto Rico dust proxy has a CIA of ~95 likely reflecting intense chemical weathering and/or abundant detrital clay minerals, as indicated by high clay-sized particle content.

4.2.2 Element-Depth Profiles

Elements considered to be relatively immobile in low-temperature and near-surface environments are commonly utilized in dust and sedimentary rock provenance studies (Cullers et al., 1979; Bhatia and Crook, 1986; McLennan, 1989; Olivarez et al., 1991; Nakai et al., 1993; Sun, 2002; Muhs et al., 2007a, 2007b; Reheis et al., 2009). We applied a Tau calculation (Eq. 1; Brimhall and Dietrich, 1987; Chadwick et al., 1990; Anderson et al., 2002) normalized to Ti and plotted results on element-depth plots to determine whether immobile elements are enriched or depleted in soil samples compared to weathered bedrock and fresh bedrock.

$$\tau_{i,j} = \frac{C_{j,w}}{C_{j,p}} \frac{C_{i,p}}{C_{i,w}} - 1 \qquad \text{Eq. 1}$$

In equation 1, C represents the concentration (ppm) of immobile (i) and mobile (j) elements in the weathered (w) and parent (p) material. Weathered material is considered all samples other than fresh bedrock. We use Ti as the immobile element because 1) it is minimally mobile in many environments (Bern et al., 2015) and 2) the concentrations of Ti in the soil samples from both Anza Borrego and Puerto Rico do not indicate signs of illuviation or leaching. When $\tau = 0$, the calculated elemental concentration in the soil matches that of the bedrock; however, if $\tau > 0$, the weathered material is enriched in that element compared to the bedrock and when $\tau < 0$, the weathered material is depleted in that element compared to bedrock. For example, a τ of -1 indicates 100% loss of the element. We plotted the elements Nb and Zr (immobile and common elements used to indicate allochthonous material), Ta and Th (commonly used in soil provenance, e.g., Muhs et al., 2007a, 2007b) and Fe and Al (typically highlight redistribution or illuviation; e.g., Chadwick et al., 1990) normalized to Ti in both Anza Borrego and Puerto Rico localities (Fig. 6).

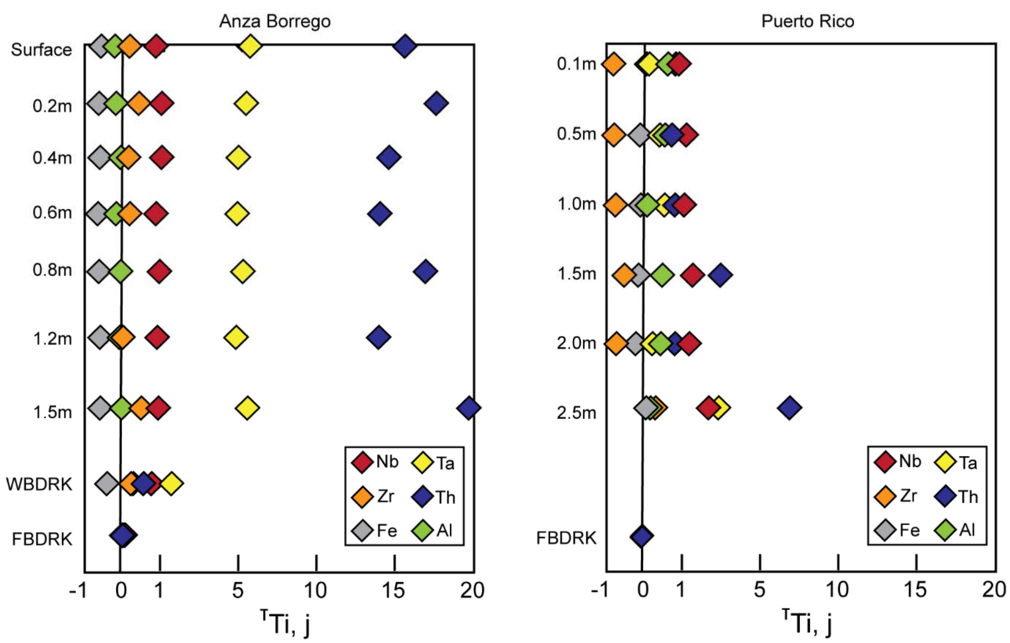

Figure 6. Tau plots showing elemental enrichment and/or depletion with depth. All elements are normalized to Ti for both Anza Borrego and Puerto Rico. Sample depth is labeled on the y-axis and depletion and enrichment values are labeled on the x-axis.

The element-depth plot for the Anza Borrego soil shows enriched values for Th, Ta, and Nb, and a slight enrichment of Zr in the soil profile samples compared to the fresh and weathered bedrock, all of which are indicative of allochthonous additions to the profile (Fig. 6; e.g., Brantley et al., 2007). The elemental enrichment values for Th and Ta are on the order of 10-20 times that of the parent material, indicating abundant accumulation of material from external sources for the mud fraction. Conversely, the Anza Borrego profile is depleted in Fe and Al compared to the bedrock samples (Fig. 6). Al is minimally depleted in the soil profile with τ-values between -0.1 – -0.2, while Fe is substantially depleted in the soil samples (τ-values = ~ -0.5) indicating almost 50% loss of Fe compared to the bedrock chemical composition. Th has the largest range of values within the soil profile with no consistent pattern between the lower and higher values. Ta, Nb, Fe, Al, and Zr values are consistent between depths within the profile. Refer to supplemental files for detailed τ-values.

Similar to the Anza Borrego profile, the Puerto Rico element-depth plot shows enriched values for Th, Ta, Nb, and Al, while Fe has an immobile pattern and Zr is almost completely depleted from the soil samples compared to the bedrock (Fig. 6). Although Zr is typically considered an immobile element, several studies have shown that the intense chemical weathering in eastern Puerto Rico causes even Zr to be mobilized (e.g., McKlintock et al., 2015; Buss et al., 2008, White, 2002) and thus depleted relative to unweathered bedrock. For this reason, we normalize to Ti for all element-depth plots in this study. In the Puerto Rico profile Fe τ-values in the upper-most samples are slightly enriched and deeper samples contain values that are slightly depleted; Zr is depleted from the uppermost portion of the profile and becomes slightly enriched in the deeper samples (Fig. 6). Notably, the highest enrichment values for all the elements occur at depths of 1.5 m and 2.5 m (Fig. 6).

4.2.3 Rare Earth Element Signatures

Rare earth element (REE; La through Lu) compositional distributions and abundances can also be used to determine provenance (e.g., Taylor and McLennan, 1995). REEs were normalized to chondritic meteorite compositions using values from Taylor and McLennan (1985). Chondrite REE patterns are expected to form smooth REE distributions; therefore, positive (enriched) and/or negative (depleted) anomalies of Ce and Eu as well as relative enrichments or depletions in the heavy REEs (HREE; Gd through Lu) and the light REEs (LREE; La through Sm) can be compared to the crystalline parent rock and dust samples to determine likely sources. The majority of REEs are contained in the clay and silt fractions, and sedimentary processes (especially granite weathering) can result in positive Ce anomalies due to the formation of Ce^{4+} and cerium hydroxides (Nesbitt, 1979; Banfield and Eggleton, 1989; Taylor and McLennon, 1995) and negative Eu anomalies via plagioclase weathering (Condie et al., 1995; Compton et al., 2003; Babechuk et al., 2014).

At the Anza Borrego locality, we plotted REE signatures for bedrock samples, dust trap sediment, and the soil profile (Fig. 7). The Anza Borrego bedrock samples have moderately low REE abundances with slightly higher LREE abundances than HREE. All three samples show slight negative Ce anomalies, and two samples show positive Eu anomalies. The Anza Borrego dust trap sediment has elevated LREE abundance, a negative Eu anomaly, and a flat distribution of HREE, but total REE abundances are higher than the bedrock samples. The soil samples all produce a consistent REE pattern that is similar to the dust trap sample, in both REE abundance and distribution.

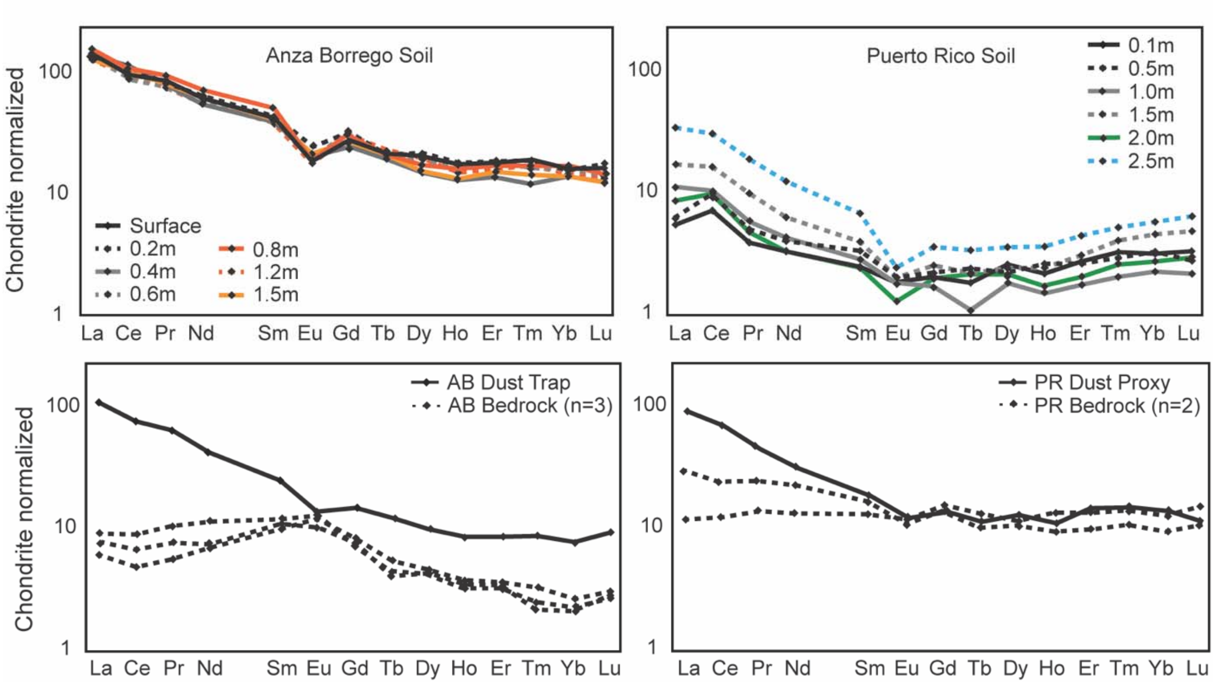

Figure 7 Chondrite-normalized REE composition and patterns of Anza Borrego (AB) and Puerto Rico (PR) soil, bedrock, dust sediment and dust proxy.

At the Puerto Rico locality, we plotted REE signatures for bedrock samples, the dust proxy sample, and the soil profile (Fig. 7). The Puerto Rico bedrock samples have relatively flat REE patterns, with similar abundances between the LREE and HREE. Both samples exhibit negative Eu anomalies and low total REE values. However, the Puerto Rico soil samples exhibit variable REE patterns. In general, samples from the deeper intervals contain higher abundances of both LREE and HREE compared to the upper-most samples; all depths have negative Eu anomalies and positive Ce anomalies. Deeper samples also resemble patterns similar to the Puerto Rico dust proxy, however with lower total abundances of REE. Near-surface samples exhibit strong positive Ce anomalies, which are not observed in either the bedrock or dust proxy samples.

5 Discussion

5.1 Intensity of Chemical Weathering

Chemical weathering and associated alteration of host material were evaluated using changes in concentrations of major elements and associated CIA values, ranges of element mobility represented in the element-depth plots, and REE patterns of the soil and bedrock samples from both localities. Unsurprisingly, all data indicate that chemical weathering is most intense in the Puerto Rico soil (Fig. 5, 6, 7). In contrast, the Anza Borrego soil shows minimal chemical weathering, consistent with low CIA values that are only slightly elevated relative to the bedrock (Fig. 5). Plagioclase weathering plays an important role at both localities, especially in initial bedrock weathering, indicated by the complete loss of the positive Eu anomaly in soil samples in Anza Borrego, despite its presence in the bedrock samples, and an increase in the intensity of the negative Eu anomaly between bedrock and soil samples in Puerto Rico (Fig. 7;

Condie et al., 1995; White et al., 1998; Compton et al., 2003; Buss et al., 2008; Babechuk et al., 2014; Joo et al., 2016, 2018). The REE observations and patterns from the mud fractions of the Anza Borrego soil samples show enrichments in the LREE, negative Eu anomalies, and overall higher abundances of REE compared to the bedrock samples. In Puerto Rico, the REE observations and patterns from the mud fractions of the soil samples include overall depleted REE abundance (both LREE and HREE), positive Ce anomalies, and more intense negative Eu anomalies (Fig. 6). Positive Ce anomalies in the soils, compared to none to slightly negative Ce anomalies in the Puerto Rico bedrock, are documented in other granitoid soils forming in humid and tropical climates (e.g., Ghani et al., 2019). The enrichment of Ce in the soil samples is likely due to the change from Ce^{3+} to Ce^{4+} due to oxidizing conditions, which is more stable and can be retained by clay minerals which are likely abundant in the Puerto Rico soils indicated by the grain size and Al-enrichment (Ghani et al., 2019).

Figure 6 shows the variations in depletion and enrichment of typically immobile elements representing chemical and biological processes at play at each locality. In Anza Borrego, both Al and Fe are slightly to moderately depleted, which is commonly associated with mineral weathering by organic (fluvic and humic) acids and/or microbial degradation (e.g., Lundström et al., 2000). Depletion of Al and Fe is a typical observation in podzols, which exhibit leaching of Fe and Al in the upper soil profile; however, podzols form in cool, humid climates with abundant vegetation (McKeague et al., 1983)— the opposite of the modern climate in the Anza Borrego Desert. The Anza Borrego profile exhibits minimal chemical weathering and minimal clay mineral content, which we would expect to result in an immobile pattern and not a depletion for these elements. Instead, we posit that this pattern likely records the influence of wetter climates of the late Pleistocene in this region (e.g., Reheis et al., 2012).

In contrast, the element-depth plots for Puerto Rico indicate leaching and associated illuviation of nearly all the plotted elements, reiterated by the low total REE abundances in the soil samples, especially in the shallow depths of the profile, all indicating mobilization of elements (Fig. 6, 7). The highest enrichment values of relatively immobile elements occur at depths of 1.5 m and 2.5 m signaling illuviation horizons, even though all depths show enrichment values for Th, Ta, Nb, and Al. Additionally, Al exhibits higher enrichment values at 0.1 m and 0.5 m depths compared to 1.0 m, which does not occur with other elements, and likely reflects dust input near the surface of the profile (Fig. 6). Fe appears to represent an immobile element in this profile, with no clear addition or depletion patterns, which could indicate bioturbation, or biogeochemical cycling (e.g., White and Buss, 2014).

The variability in chemical weathering and subsequent element mobility between the two localities is expected given the order-of-magnitude larger mean-annual precipitation and higher mean-annual temperature in Puerto Rico compared to Anza Borrego. This difference likely impacts the resulting silt generation in each profile, which partly explains the extremely low volumes of silt and clay in Anza Borrego and abundance of silt and clay in the Puerto Rico soil. Additionally, the finer initial crystal size of the Puerto Rico bedrock likely contributes to the efficacy of chemical (and physical) weathering in creating the abundant mud fraction observed in these samples. In contrast, it seems unlikely that the silt in Anza Borrego formed from bedrock weathering— either chemically or physically— as explored further below.

5.2 Evidence for Dust Additions

The role of soil as a trap for dust is well recognized (e.g., Yaalon and Ganor, 1973; review by Muhs, 2013); indeed, dust can deliver significant macro- and micronutrients to soil ecosystems. Dust can contribute significant volumes of fine-grained material to soils depending on their geographic proximity to potential dust sources, and many studies have documented additions of long-range-traveled (LRT) dust to soils (e.g., Birkeland, 1999; Kurtz et al., 2001; Muhs et al., 2021) including in the Caribbean Islands (e.g., Muhs et al., 2007b; Pett-Ridge, 2009; Pett-Ridge et al., 2009; McClintock et al., 2015, 2019) and southern California (Muhs et al., 2007a, 2008; Reheis et al., 2009). Ultimately, soils developed on coarse-grained host rocks can produce some autochthonous silt via pedogenic weathering but can also contain allochthonous silt attributable to local dust inputs. These processes are potentially distinguishable by comparing particle size and geochemical attributes of the soils relative to parent rock and dust sources.

Both study profiles follow expected grain-size distribution patterns: the Anza Borrego soil is predominately sand, representing a more arenaceous profile common in temperate climates (e.g., Hall, 1985; 1987), and the Puerto Rico profile is predominately mud, especially very-fine silt and clay, representing an argillaceous profile more expected in humid climates (Fig. 4, Table 2). The distribution of grain sizes in each profile largely reflects the significant contrast in intensity of chemical weathering, as well as differences in eolian inputs. In addition to the A-CN-K diagram and element-depth plots, we plot elements with low expected mobility, Nd-Cr-Ta and Th-La-Sc (Taylor and McLennon, 1985; Olivarez et al., 1991; Muhs et al., 2007b, 2021) on ternary diagrams to further investigate the provenance of the mud fraction (cf., Muhs and Budahn, 2009; Muhs et al., 2007b, 2010, 2021; Reheis et al., 2009). Figure 8 compares data from this study and potential dust source fields from previous works by Muhs et al. (2007b) and Reheis (2003).

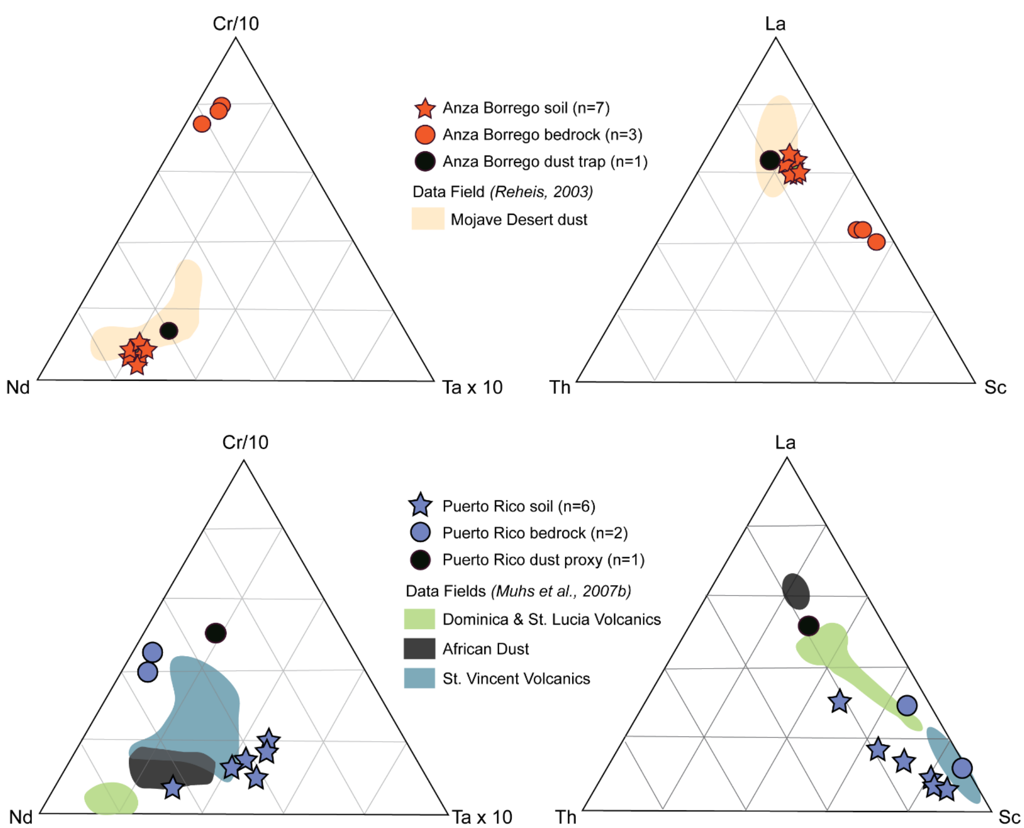

Figure 8. Cr/10 - Nd - Tax10 and La - Th - Sc ternary diagrams of Anza Borrego and Puerto Rico samples compared to previously published data of Mojave Desert dust (Reheis, 2003), Lesser Antilles volcanic system (Turner et al., 1996; Heath et al., 1998; Muhs et al., 2007b), and African dust (Muhs et al., 2007b). These diagrams show that the mud-fraction from the Anza Borrego soil is geochemically indistinguishable from dust sources and the Puerto Rico soil is largely affected by chemical weathering, making it fall between potential sources.

The Anza Borrego dust trap sediment exhibits bulk geochemistry which likely reflects a mafic source. The addition of dust to the Anza Borrego profile could influence the geochemical signature of the soils, potentially shifting to lower CIA values, for example (Fig. 5, 7; discussion above). The REE signatures of the soil samples from Anza Borrego and the dust trap samples are comparable and plot similarly to other Greater Mojave Desert dust samples within the region (Fig. 7; e.g., Reheis et al., 2002). The dust trap sample we analyzed from Reheis and Kihl (1995) (T59; that was not influenced by mica) reported a mode of 32 μm which aligns with the data observed in the soil profile and is consistent with other studies. Emery (1960) reported dust from Santa Ana wind events collected in Los Angeles as having grain-size modes between 30 – 40 μm, comparable to the modes of the mud fraction in the Anza Borrego soil (Fig. 9). Additionally, Reynolds et al., (2006) reported silt contents from dust traps around the Greater Mojave Desert region as predominantly coarse silt (up to 55%), also aligning with the granulometric results from the Anza Borrego soil profile. Figure 8 illustrates that the geochemical signatures from the mud fractions of the soil samples and the dust trap data plot within the Greater Mojave Desert dust provenance fields reported by Reheis (2003) and Reheis et al. (2002). Within Nd-Cr-Ta space, the soil samples cluster near the Nd apex along with the dust trap sample, all of which fall within the Greater Mojave Desert dust field; similarly, in Th-La-Sc space the soil samples and dust trap sediment create a distinct cluster near the La apex within the Greater Mojave Desert dust field. Additionally, the bedrock samples plot in separate clusters closer to the Cr apex in Nd-Cr-Ta space and towards the Sc apex in Th-La-Sc space. Figure 6 also shows evidence for allochthonous additions to the Anza Borrego profile with enrichment values upwards of 15 for Th and well above 1 for Ta and Nb. These data reinforce the interpretation of a predominantly allochthonous, eolian origin for the mud fraction of the Anza Borrego soil, rather than an *in situ* origin by pedogenic weathering of the parent material.

The Puerto Rico dust proxy is predominantly clay with a very-fine mode of 5 μm, which is also consistent with LRT dust likely from the North African Saharan or Sahel deserts or the Lesser Antilles volcanic arc system (Fig. 4). Although the only soil depth that aligns granulometrically with the dust proxy occurs at 0.5-m, the top two meters of the Puerto Rico profile display bimodal histograms with both ~5 and 18 μm modes (Fig. 4). This bimodal distribution is consistent with the possibility of multiple sources for the fines in this profile – e.g. autochthonous production of clays by weathering, and allochthonous input of LRT dust. Since the lower depths are more consistently coarse, we posit that the majority of the coarser mode of 18 μm represents the autochthonous silt fraction produced via pedogenic weathering, while the 5 μm mode likely represents (at least partially) the LRT dust fraction, as typical grain-sizes of African dust particles are 2.5 – 5 μm (Fig. 9; Li-Jones and Prospero, 1998). Examples from distal ash falls from Dominica range in grain size from coarse silt (45 μm) to fine silt (14 μm); however more proximal ashfall would be coarser (Carey and Sigurdsson, 1980). Grain size decreases with distance from an eruption, so we assume that any dust that reached Puerto Rico would be in the coarse silt range (Carey and Sigurdsson; 1980), consistent with the proximity of the arc.

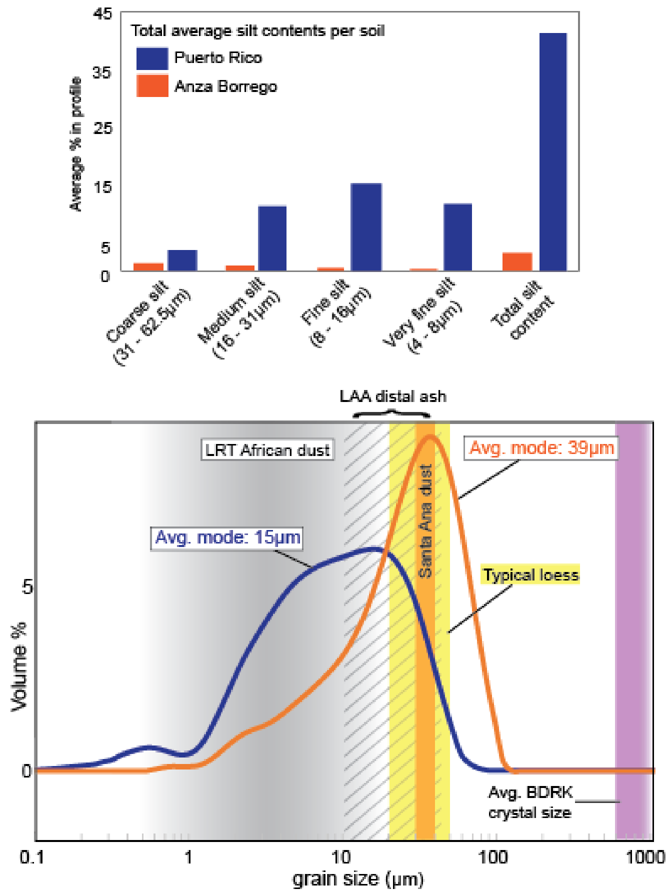

Figure 9. Average total silt contents in each soil profile (above) and grain size distributions compared to potential dust sources (below) for the two localities. The annotated histogram-plot of grain size distributions for the average soil (Puerto Rico in blue, Anza Borrego in orange) compared to typical loess modes (yellow), typical grain size collected in Santa Ana dust (orange), reported Lesser Antilles Arc (LAA, gray diagonal lines) grain sizes for distal ash, and reported LRT African dust (gray) grain sizes. The representative average bedrock crystal size from thin section observations is shown in purple. The range of typical loess grain size falls directly between the soil modes, and the bedrock-host crystals are substantially coarser than both the soil and a typical loess deposit. However, there is a strong overlap in grain size between Santa Ana dust and the Anza Borrego soil. Similarly, the Puerto Rico soil overlaps with LRT African dust and LAA distal ash.

Similar to Anza Borrego, Puerto Rico soil samples also exhibit enriched values for multiple immobile elements including Nb, Ta, Th, and Al indicating external sources for the mud fraction (Fig. 6). Additions of volcanic and clay minerals from dust sources likely contribute to the high CIA values in the dust proxy as well as the enrichment of Al in the element-depth plots. However, unlike the comparable attributes observed between the Anza Borrego dust sediment and soils, the Puerto Rico dust proxy does not align entirely with the soil samples in Puerto Rico, as shown in Figure 8. Interestingly, the dust proxy plots in between the values for the provenance of African dust, Dominica and St. Lucia volcanics (Muhs et al., 2007b) on the Th-La-Sc ternary plot, but plots closer to the St. Vincent volcanics provenance field in the Nd-Cr-Ta ternary plot. In the Th-La-Sc plot, the soil samples fall near a mixing line between the bedrock samples and the dust proxy data point, plotting near the volcanic provenance fields, but not overlapping. In the Nd-Cr-Sc plot, the bedrock and dust proxy samples do not align with the soil samples, but a few of the soil samples overlap with St. Vincent volcanics and African dust. Overall, the soil samples produce irregular signatures with regards to dust data fields, but the Th-La-Sc plot indicates a strong African dust influence, while the Nd-Cr-Ta plot indicates a mix of potential sources.

In summary, geochemical evidence from both localities are consistent with the influence of allochthonous dust to the soil profiles, despite the lack of eolian mantles apparent in the A horizons (the uppermost part of the profile, e.g., Yaalon and Ganor, 1973). The data support an almost entirely dust-derived silt fraction in Anza Borrego, and a completely homogenized silt fraction mixed with both parent rock and dust inputs in Puerto Rico, regardless of sample depth.

5.3 Implications for Loess Formation

To examine the efficacy of pedogenic weathering (by physical, chemical, and biological processes) as a major mechanism for silt generation, we evaluate the results from both profiles within the context of critical attributes of geologically significant loess deposits. At the broadest scale, these factors include 1) the grain-size mode of the silt fraction in each soil profile compared to typical loess modes and 2) the amount of silt contained in the soil compared to the volume of silt in a loess deposit. Note that we focus not only on the mode and volume of silt-sized quartz, but on all the silt-sized mineral constituents within the mud fraction of each soil. Although loess is commonly dominated by quartz silt, most loess deposits contain varying amounts of quartz, plagioclase, K-feldspar, carbonate minerals, mica, and phyllosilicate clay minerals including chlorite, illite, kaolinite, and smectite (e.g., Tsoar and Pye, 1987; Muhs, 2013). The profiles in Puerto Rico and Anza Borrego were evaluated holistically in order to achieve a broader understanding of the attributes of the extant silt.

Soil particle size distribution hinges to a large degree on grain- or crystal-size within the parent material. For example, a soil profile forming on loess, or on a siltstone, phyllite, or tuff is likely silt rich due to the abundant silt available in the host. In contrast, particle size trends within granitoid-hosted weathering profiles exhibit a predominance of sand with minimal silt and clay (e.g., Hoskin and Sundeen, 1985; Dixon and Young, 1981; Wang et al., 1981; Taboada and Garcia, 1999; Wright, 2002a, 2002b), indicating that typical weathering profiles formed from coarse-grained parent material do not contain significant amounts of autochthonous silt. The weathering profiles from Anza Borrego and Puerto Rico both formed from granitoid bedrock, enabling assessment of the efficacy of pedogenic weathering in creating silt from grains typically coarser than 0.5 mm diameter (Fig. 2; Table 3).

Loess deposits are reported to have “typical” grain size modes of 20 – 40 μm (e.g., Tsoar and Pye, 1987; Assallay et al., 1998; Anderson, 2007), although some authors report modes of up to 50 μm (e.g., Smalley and Krinsley, 1978). Modes vary owing to distance from sources and predominant wind velocities, among other factors. For example, Chinese loess exhibits a typical mode of ~25 μm (e.g., Assalley et al., 1998; Lu et al., 2001) although more proximal deposits are coarser than the distal loess (e.g., Ding et al., 2001), the Peoria loess (midwest U.S.) has an average mode of ~40 μm (Wang et al., 2006), and the Negev loess (Israel) is bimodal, with a coarse (50 – 60 μm) and fine (<10 μm) mode (Crouvi et al., 2008). Regardless, it's widely agreed that typical modes fall within the medium and coarse silt range, with very few studies reporting geologically significant loess or loess-like deposits with modes in the fine silt range (e.g., Pfeifer et al., 2020).

Medium (16 – 31 μm) and coarse (31 – 62.5 μm) silt accounts for about 20% of the Puerto Rico soil, and <3% of the Anza Borrego soil (Table 2; Fig. 9). Ultimately, neither the Anza Borrego nor Puerto Rico soils contain a significant volume of silt in the typical loess ranges discussed above; the Anza Borrego mud-fraction mode (40 μm) is relatively coarse, but constitutes a negligible amount by volume, and the Puerto Rico mud-fraction is skewed finer (5 – 18 μm) relative to the typical grain size modes observed in loess deposits throughout geologic time (Fig. 9). For comparison, Nahon and Trompette (1982) reported quartz and feldspar fragments between 1 and 20 μm diameter in the soils from their original study when proposing that abundant silt was produced by pedogenic weathering. These diameters are smaller than the typical loess size modes (typically > 20μm; references above), but similar to the results of the tropical soil profile from Puerto Rico where the majority of the soil was clay to fine silt.

If soil weathering is an efficacious mechanism to generate the silt that forms loess, it must produce silt in modes similar to (or larger than) those of typical loess in sufficient volumes of this material to result in a loess deposit. We can evaluate the efficiency of silt production by considering the maximum silt contents in each soil profile (e.g., Anza Borrego: 5%; Puerto Rico: 50% of total soil) assuming development of a mature, 10-m profile thickness, and assess the area needed to source a small (e.g. Negev) or large (e.g. Chinese) loess deposit. The Negev loess, a relatively small accumulation, covers ~5,500 km^2 with an average thickness of ~10 meters (Crouvi et al., 2008; Ben-Israel et al., 2015). The Chinese Loess Plateau (CLP) is the largest loess accumulation on Earth today, at 640,000 km^2 with an average mean thickness of ~100 meters (e.g., Zhu et al., 2018).

$$(area\ of\ soil\ km^2 \times thickness\ of\ soil\ km) \times \%\ silt\ in\ soil = volume\ of\ loess\ km^3 \qquad \text{Eq. 2}$$

Using equation 2, in order to generate sufficient silt to form the Negev loess, a soil comparable to Puerto Rico would need to cover an area about twice the size of the loess deposit (~11,000 km^2) and a soil comparable to Anza Borrego would need to cover 20-times the area of the loess (~110,000 km^2). To supply the likes of the Chinese Loess Plateau, a soil with silt contents similar to Puerto Rico would need to cover 20-times the area of the CLP (about 12.8 million km^2; about 2-times the land area of Russia) and a soil similar to the Anza Borrego profile would need to cover an area 200-times that of the loess plateau (128 million km^2; approximately 25% of the Earth's total land area). These are conservative estimates, since 1) we assume use of the entire silt fraction and not just the fractions of the typical loess modes and 2) a soil profile formed in a climate like the Anza Borrego Desert is unlikely to reach a thickness of 10 m. Additionally, these profiles would need to be reworked to release all of their silt, then undergo additional transport and sedimentation processes to isolate the silt-size grains, eventually to be deposited at an accumulation site. For comparison, experimental studies have shown that sand saltation as a means for silt generation for desert loess would require a primary dune field 85-times larger than the accumulated loess deposit (Adams and Soreghan, 2020).

The Anza Borrego profile contains insignificant volumes of silt. Thus, the Anza Borrego profile cannot be a major source of silt for loess generation, particularly given that geochemical results indicate that the little silt observed in this soil is likely completely derived from eolian transport. Conversely, the Puerto Rico soil contains significant silt, enough to be reworked and deposited to form a major loess deposit. However, the largest mode (18μm) is finer than the lower end of the typical loess mode range proposed in literature (Smalley and Krinsley, 1978; Tsoar and Pye, 1987; Assallay et al., 1998; Anderson, 2007).

6. Conclusions

Pedogenic weathering in hot (tropical and Mediterranean) climates has been long cited as an effective means for silt generation to source loess, but this hypothesis has not been tested rigorously. The efficacy of pedogenic weathering in the production of silt is important for constraining potential climatic and environmental interpretations of loess deposits, especially in deep time. Granulometric and geochemical data from soils in tropical hot-humid (Puerto Rico) and Mediterranean hot-arid (Anza Borrego) localities contrast greatly, despite formation on similar granitoid-derived bedrock material. The soil profile from Anza Borrego contains insufficient silt to form a geologically significant loess deposit, and much of the silt that is present was likely delivered via eolian processes and was not formed in-situ. The Puerto Rico soil generates autochthonous silt *in situ*, and also incorporates allochthonous silt and clay from eolian additions, but the modes tend to be finer than typical loess modes. Intense pedogenic weathering in wet and hot climates could account for portions of silt distributions throughout geologic time, and merits further study to quantitatively decipher the source of the silt, as well as the mineralogy of the silt, and the volume of silt produced within a typical weathering profile. However, in general, unrealistically large volumes of soil would be needed to generate significant loess deposits. Future studies must consider the mechanisms needed to release and rework the grains within these weathering profiles and the geographic locations of modern and ancient loess in relation to tropically weathered soil profiles.

(All figures and tables should be cited in order. For initial submission, please embed figures, tables, and their captions within the main text near where they are cited. At revision, figures should be uploaded separately, as we need separate files for production. Tables and all captions should be moved to the end of the file.)

Acknowledgments

This research was supported by the U.S. National Science Foundation (NSF) grant # 1543344.

Thank you to N. Webb and Y.J. Joo for sample collection and assistance with data collection.

Thank you to M. Reheis for discussion related to this work and her generosity in sharing her Anza Borrego Desert dust samples for additional analyses. We thank C. Floyd and C. Hodges for additional discussions regarding data and research-related questions.

Open Research

This research was conducted using geochemical data and granulometric data. All software used in analysis and data visualization are available to the public: imageJ, adobe illustrator, and Microsoft excel. For peer review, raw data files have been provided in the supplementary information of this paper. Raw data files are in the process of being made publically accessible in a general repository and access will be described here prior to publication acceptance.

References

Adams, S. M., & Soreghan, G. S. (2020). A test of the efficacy of sand saltation for silt production: Implications for the interpretation of loess. *Geology*, *48*(11), 1105–1109. https://doi.org/10.1130/G47282.1

Anderson, S. P. (2007). Biogeochemistry of glacial landscape systems. *Annual Review of Earth and Planetary Sciences*, *35*(1), 375-399.

Anderson, S. P., Dietrich, W. E., & Brimhall Jr, G. H. (2002). Weathering profiles, mass-balance analysis, and rates of solute loss: Linkages between weathering and erosion in a small, steep catchment. *Geological Society of America Bulletin*, *114*(9), 1143-1158.

Assallay, A. M., Rogers, C. D. F., Smalley, I. J., & Jefferson, I. F. (1998). Silt: 2-62 μm, 9-4φ. *Earth Science Reviews*, *45*(1–2), 61–88. https://doi.org/10.1016/S0012-8252(98)00035-X

Babechuk, M. G., Widdowson, M., & Kamber, B. S. (2014). Quantifying chemical weathering intensity and trace element release from two contrasting basalt profiles, Deccan Traps, India. *Chemical Geology*, *363*, 56-75.

Banfield, J. F., & Eggleton, R. A. (1989). Apatite replacement and rare earth mobilization, fractionation, and fixation during weathering. *Clays and Clay Minerals*, *37*(2), 113-127.

Beck, H. E., Zimmermann, N. E., McVicar, T. R., Vergopolan, N., Berg, A., & Wood, E. F. (2018). Present and future köppen-geiger climate classification maps at 1-km resolution. *Scientific Data*, *5*, 1–12. https://doi.org/10.1038/sdata.2018.214

Ben-Israel, M., Enzel, Y., Amit, R., & Erel, Y. (2015). Provenance of the various grain-size fractions in the Negev loess and potential changes in major dust sources to the Eastern Mediterranean. *Quaternary Research*, *83*(1), 105-115.

Bern, C. R., Thompson, A., & Chadwick, O. A. (2015). Quantification of colloidal and aqueous element transfer in soils: The dual-phase mass balance model. *Geochimica et Cosmochimica Acta*, *151*, 1-18.

Bhatia, M. R., & Crook, K. A. (1986). Trace element characteristics of graywackes and tectonic setting discrimination of sedimentary basins. *Contributions to mineralogy and petrology*, *92*(2), 181-193.

Birkeland, P. W. (1984). *Soils and geomorphology*. Oxford university press.

Blisniuk, K., Oskin, M., Fletcher, K., Rockwell, T. & Sharp, W. (2012). Assessing the reliability of U-series and 10 Be dating techniques on alluvial fans in the Anza Borrego Desert, California. *Quaternary Geochronology, 13*, 26–41.

Brantley, S. L., Goldhaber, M. B., & Vala Ragnarsdottir, K. (2007). Crossing disciplines and scales to understand the critical zone. *Elements*, *3*(5), 307–314. https://doi.org/10.2113/gselements.3.5.307

Braun, J. J., Viers, J., Dupré, B., Polve, M., Ndam, J., & Muller, J. P. (1998). Solid/liquid REE fractionation in the lateritic system of Goyoum, East Cameroon: the implication for the present dynamics of the soil covers of the humid tropical regions. *Geochimica et Cosmochimica Acta*, *62*(2), 273-299.

Brimhall, G. H., & Dietrich, W. E. (1987). Constitutive mass balance relations between chemical composition, volume, density, porosity, and strain in metasomatic hydrochemical systems: results on weathering and pedogenesis. *Geochimica et Cosmochimica Acta*, *51*(3), 567-587.

Buss, H. L., Sak, P. B., Webb, S. M., & Brantley, S. L. (2008). Weathering of the Rio Blanco quartz diorite, Luquillo Mountains, Puerto Rico: Coupling oxidation, dissolution, and fracturing. *Geochimica et Cosmochimica Acta*, *72*(18), 4488–4507. https://doi.org/10.1016/j.gca.2008.06.020

Carey, S. N., & Sigurdsson, H. (1978). Deep-sea evidence for distribution of tephra from the mixed magma eruption of the Soufrière on St. Vincent, 1902: Ash turbidites and air fall. *Geology*, *6*(5), 271–274.

Carey, S. N., & Sigurdsson, H. (1980). The Roseau ash: Deep-sea tephra deposits from a major eruption on Dominica, Lesser Antilles arc. *Journal of Volcanology and Geothermal Research*, *7*(1–2), 67–86. https://doi.org/10.1016/0377-0273(80)90020-7

Catt, J. A. (1988). Loess—its formation, transport and economic significance. In *Physical and chemical weathering in geochemical cycles* (pp. 113-142). Springer, Dordrecht.

Chadwick, O. A., Brimhall, G. H., & Hendricks, D. M. (1990). From a black to a gray box - a mass balance interpretation of pedogenesis. *Geomorphology*, *3*(3–4), 369–390. https://doi.org/10.1016/0169-555X(90)90012-F

Clinkenbeard, J. P., & Walawender, M. J. (1989). Mineralogy of the La Posta pluton: Implications for the origin of zoned plutons in the eastern Peninsular Ranges batholith, southern and Baja California. *American Mineralogist, 74*(11-12), 1258-1269.

Compton, J. S., White, R. A., & Smith, M. (2003). Rare earth element behavior in soils and salt pan sediments of a semi-arid granitic terrain in the Western Cape, South Africa. *Chemical Geology*, *201*(3-4), 239-255.

Condie, K. C., Dengate, J., & Cullers, R. L. (1995). Behavior of rare earth elements in a paleoweathering profile on granodiorite in the Front Range, Colorado, USA. *Geochimica et Cosmochimica Acta*, *59*(2), 279-294.

Crouvi, O., Amit, R., Enzel, Y., Porat, N., & Sandler, A. (2008). Sand dunes as a major proximal dust source for late Pleistocene loess in the Negev Desert, Israel. *Quaternary Research*, *70*(2), 275–282. https://doi.org/10.1016/j.yqres.2008.04.011

Cullers, R., Chaudhuri, S., Kilbane, N., & Koch, R. (1979). Rare-earths in size fractions and sedimentary rocks of Pennsylvanian-Permian age from the mid-continent of the USA. *Geochimica et Cosmochimica Acta*, *43*(8), 1285-1301.

Dixon, J. C., & Young, R. W. (1981). Character and origin of deep arenaceous weathering mantles on the Bega Batholith, southeastern Australia. *Catena*, *8*(1), 97-109.

Emery, K. O. (1960). *The sea off southern California, a modern habitat of petroleum*. John Wiley and Sons, Inc.

Enzel, Y., Amit, R., Crouvi, O., & Porat, N. (2010). Abrasion-derived sediments under intensified winds at the latest Pleistocene leading edge of the advancing Sinai-Negev erg. *Quaternary Research, 74,* 121–131, https://doi .org/10.1016/j.yqres.2010.04.002

Fletcher, K. E., Rockwell, T. K., & Sharp, W. D. (2011). Late Quaternary slip rate of the southern Elsinore fault, Southern California: Dating offset alluvial fans via 230Th/U on pedogenic carbonate. *Journal of Geophysical Research: Earth Surface, 116*(F2). doi:10.1029/2010JF001701

Frey, H., Schmidt, A., Joseph, E., & Waters, L. (2018). Hazards in the Caribbean: the History of Magma Chambers, Eruptions, Landslides, Streams, and Fumeroles in Dominica. *Short Contributions KECK Geology Consortium*, *31*, 1–12.

Ghani, A. A., Muzammil, S., Ng, T. F., Noer, E. H. I., Mohamad, T. M. Z., Nur, I., et al. (2019). Ce Anomaly in I–Type Granitic Soil from Kuantan, Peninsular Malaysia: Retention of Zircon in the Weathering Product. *Sains Malaysiana*, *48*(2), 309-315.

Glaccum, R. A., & Prospero, J. M. (1980). Saharan aerosols over the tropical North Atlantic—Mineralogy. *Marine geology, 37*(3-4), 295-321.

Hall, A. M. (1985). Cenozoic weathering covers in Buchan, Scotland and their significance. *Nature*, *315*(6018), 392-395.

Hall, A. M. (1987). Deep weathering patterns in north-east Scotland and their geomorphological significance. *Zeitschrift für Geomorphologie*, 407-422.

Heath, E., Macdonald, R., Belkin, H., Hawkesworth, C., & Sigurdsson, H. (1998). Magmagenesis at Soufriere Volcano, St Vincent, Lesser Antilles Arc. *Journal of Petrology*, *39*(10), 1721-1764.

Hoskin, C. M., & Sundeen, D. A. (1985). Grain size of granite and derived grus, Enchanted Rock pluton, Texas. *Sedimentary geology*, *42*(1-2), 25-40.

Johnson, M. R., (1994). Thin section grain size analysis revisited. *Sedimentology, 41,* 985–999. https://doi.org/10.1111/j.1365-3091.1994.tb01436.x

Joo, Y. J., Madden, M. E. E., & Soreghan, G. S. (2016). Chemical and physical weathering in a hot-arid, tectonically active alluvial system of Anza Borrego desert, California. *Sedimentology*, *63*(5), 1065–1083. https://doi.org/10.1111/sed.12249

Joo, Y. J., Madden, M. E. E. E., & Soreghan, G. S. (2018). Anomalously low chemical weathering in fluvial sediment of a tropical watershed (Puerto Rico). *Geology*, *46*(8), 691–694. https://doi.org/10.1130/G40315.1

Kuenen, P.H. (1960). Experimental abrasion 4: Eolian action*: The Journal of Geology, 68,* 427–449.

Kurtz, A. C., Derry, L. A., & Chadwick, O. A. (2001). Accretion of Asian dust to Hawaiian soils: isotopic, elemental, and mineral mass balances. *Geochimica et Cosmochimica acta*, *65*(12), 1971-1983.

Lau, K. M., & Kim, K. M. (2007). Cooling of the Atlantic by Saharan dust. *Geophysical Research Letters*, *34*(23), 8–11. https://doi.org/10.1029/2007GL031538

Le Friant, A., Lock, E. J., Hart, M. B., Boudon, G., Sparks, R. S. J., Leng, M. J., et al. (2008). Late Pleistocene tephrochronology of marine sediments adjacent to Montserrat, Lesser Antilles volcanic arc. *Journal of the Geological Society*, *165*(1), 279–289. https://doi.org/10.1144/0016-76492007-019

Li, Y., Shi, W., Aydin, A., Beroya-Eitner, M. A., & Gao, G. (2020). Loess genesis and worldwide distribution. *Earth-Science Reviews*, *201*, 102947. https://doi.org/10.1016/j.earscirev.2019.102947

Li-Jones, X., & Prospero, J. M. (1998). Variations in the size distribution of non-sea-salt sulfate aerosol in the marine boundary layer at Barbados: Impact of African dust. *Journal of Geophysical Research: Atmospheres*, *103*(D13), 16073-16084.

Lu, H., Vandenberghe, J., & An, Z. (2001). Aeolian origin and palaeoclimatic implications of the 'red clay' (north China) as evidenced by grain-size distribution. *Journal of Quaternary Science: Published for the Quaternary Research Association*, *16*(1), 89-97.

Lundström, U. S., Van Breemen, N., & Bain, D. (2000). The podzolization process. A review. *Geoderma*, *94*(2-4), 91-107.

McClintock, M. A., Brocard, G., Willenbring, J., Tamayo, C., Porder, S., & Pett-Ridge, J. C. (2015). Spatial variability of African dust in soils in a montane tropical landscape in Puerto Rico. *Chemical Geology*, *412*, 69-81.

McClintock, M. A., McDowell, W. H., González, G., Schulz, M., & Pett-Ridge, J. C. (2019). African dust deposition in Puerto Rico: Analysis of a 20-year rainfall chemistry record and comparison with models. *Atmospheric Environment*, *216*, 116907.

McKeague, J. A., De Connick, F., & Franzmeier, D. P. (1983). Spodsols. In: Wilding, L. P., Smeck, Ž. N. E., Hall, G. F. (Eds.), *Pedogenesis and Soil Taxonomy*. (217–252). Elsevier, New York.

McLennan, S. M. (1989). Rare earth elements in sedimentary rocks: Influence of provenance and sedimentary processes. *Mineralogical Society of America Reviews in Mineralogy, 21*, 169-200.

Moss, A. J. (1966). Origin, shaping and significance of quartz sand grains. *Journal of the Geological Society of Australia*, *13*(1), https://doi.org/10.1080/00167616608728607

Moss, A. J., & Green, P. (1975). Sand and silt grains: Predetermination of their formation and properties by microfractures in quartz. *Journal of the Geological Society of Australia*, *22*(4), 485–495. https://doi.org/10.1080/00167617508728913

Muhs, D. R. (1983). Airborne dust fall on the California Channel Islands, U.S.A (Mojave Desert). *Journal of Arid Environments*, *6*(3), 223–238. https://doi.org/10.1016/s0140-1963(18)31507-6

Muhs, D. R. (2013). The geologic records of dust in the Quaternary. *Aeolian Research*, *9*, 3–48.

Muhs, D. R., & Bettis, E. A. (2003). Quaternary loess-paleosol sequences as examples of climate-driven sedimentary extremes. *Special Paper of the Geological Society of America*, *370*(303), 53–74. https://doi.org/10.1130/0-8137-2370-1.53

Muhs, D. R., & Budahn, J. R. (2009). Geochemical evidence for African dust and volcanic ash inputs to terra rossa soils on carbonate reef terraces, northern Jamaica, West Indies. *Quaternary International*, *196*(1–2), 13–35. https://doi.org/10.1016/j.quaint.2007.10.026

Muhs, D. R., Budahn, J., Reheis, M., Beann, J., Skipp, G., & Fisher, E. (2007a). Airborne dust transport to the eastern Pacific Ocean off southern California: Evidence from San Clemente Island. *Journal of Geophysical Research Atmospheres*, *112*(13), 1–17. https://doi.org/10.1029/2006JD007577

Muhs, D. R., Budahn, J. R., Prospero, J. M., & Carey, S. N. (2007b). Geochemical evidence for African dust inputs to soils of western Atlantic islands: Barbados, the Bahamas, and Florida. *Journal of Geophysical Research: Earth Surface*, *112*(2), 1–26. https://doi.org/10.1029/2005JF000445

Muhs, D. R., Budahn, J. R., Johnson, D. L., Reheis, M., Beann, J., Skipp, G., et al. (2008). Geochemical evidence for airborne dust additions to soils in Channel Islands National Park, California. *Bulletin of the Geological Society of America*, *120*(1–2), 106–126. https://doi.org/10.1130/B26218.1

Muhs, D. R., Cattle, S. R., Crouvi, O., Rousseau, D. D., Sun, J., & Zárate, M. A. (2014). Loess records. In *Mineral Dust* (411-441). Springer, Dordrecht.

Muhs, D. R., Meco, J., Budahn, J. R., Skipp, G. L., Simmons, K. R., Baddock, M. C., et al. (2021). Long-term African dust delivery to the eastern Atlantic Ocean from the Sahara and Sahel regions: Evidence from Quaternary paleosols on the Canary Islands, Spain. *Quaternary Science Reviews*, *265*, 107024. https://doi.org/10.1016/j.quascirev.2021.107024

Nahon, D., & Trompette, R. (1982). Origin of siltstones: glacial grinding versus weathering. *Sedimentology*, *29*(1), 25–35. https://doi.org/10.1111/j.1365-3091.1982.tb01706.x

Nakai, S. I., Halliday, A. N., & Rea, D. K. (1993). Provenance of dust in the Pacific Ocean. *Earth and Planetary Science Letters*, *119*(1-2), 143-157.

Nesbitt, H. W. (1979). Mobility and fractionation of rare earth elements during weathering of a granodiorite. *Nature*, *279*(5710), 206-210.

Nesbitt, H., & Young, G. M. (1982). Early Proterozoic climates and plate motions inferred from major element chemistry of lutites. *Nature*, *299*(5885), 715-717.

Nesbitt, H. W., & Young, G. M. (1984). Prediction of some weathering trends of plutonic and volcanic rocks based on thermodynamic and kinetic considerations. *Geochimica et Cosmochimica Acta*, *48*(7), 1523–1534. https://doi.org/10.1016/0016-7037(84)90408-3

Nesbitt, H. W., & Young, G. M. (1989). Formation and diagenesis of weathering profiles. *The Journal of Geology*, *97*(2), 129-147.

NOAA Climate Normals. (2021). Latest 30 year period 1991-2020, National Centers for Environmental Information. U.S. Climate Normals Quick Access Station Borrego Desert Park. NOAA NCEI U.S. Climate Normals Quick Access

NOAA Climate Normals. (2021). Latest 30 year period 1991-2020, National Centers for Environmental Information. U.S. Climate Normals Quick Access Station Guayama 2E. NOAA NCEI U.S. Climate Normals Quick Access

Olivarez, A. M., Owen, R. M., & Rea, D. K. (1991). Geochemistry of eolian dust in Pacific pelagic sediments: Implications for paleoclimatic interpretations. *Geochimica et Cosmochimica Acta*, *55*(8), 2147-2158.

Pfeifer, L. S., Soreghan, G. S., Pochat, S., & Van Den Driessche, J. (2021). Loess in eastern equatorial Pangea archives a dusty atmosphere and possible upland glaciation. *GSA Bulletin*, *133*(1-2), 379-392.

Prospero, J. M., Bonatti, E., Schubert, C., & Carlson, T. N. (1970). Dust in the Caribbean atmosphere traced to an African dust storm. *Earth and Planetary Science Letters*, *9*(3), 287–293. https://doi.org/10.1016/0012-821X(70)90039-7

Prospero, J. M., & Lamb, P. J. (2003). African Droughts and Dust Transport to the Caribbean: Climate Change Implications. *Science*, *302*(5647), 1024–1027. https://doi.org/10.1126/science.1089915

Pye, K. (1995). The nature, origin and accumulation of loess. *Quaternary Science Reviews*, *14*(7–8), 653–667. https://doi.org/10.1016/0277-3791(95)00047-X

Pye, K., & Sperling, C. H. B. (1983). Experimental investigation of silt formation by static breakage processes: the effect of temperature, moisture and salt on quartz dune sand and granitic regolith. *Sedimentology*, *30*(1), 49–62. https://doi.org/10.1111/j.1365-3091.1983.tb00649.x

Pett-Ridge, J. C. (2009). Contributions of dust to phosphorus cycling in tropical forests of the Luquillo Mountains, Puerto Rico. *Biogeochemistry*, *94*(1), 63–80. https://doi.org/10.1007/s10533-009-9308-x

Pett-Ridge, J. C., Derry, L. A., & Kurtz, A. C. (2009). Sr isotopes as a tracer of weathering processes and dust inputs in a tropical granitoid watershed, Luquillo Mountains, Puerto Rico. *Geochimica et Cosmochimica Acta*, *73*(1), 25–43. https://doi.org/10.1016/j.gca.2008.09.032

Reheis, M.C. (2003). Dust deposition in Nevada, California, and Utah, 1984–2002. *US Geological Survey Open-File Report 03-138.*

Reheis, M. C., & Kihl, R. (1995). Dust deposition in southern Nevada and California, USA 1984-1989: relations to climate, source area and source lithology. *Journal of Geophysical Research, 100*, 8893–8918. DOI: 10.1029/94JD03245

Reheis, M. C., Goodmacher, J. C., Hardem, J. W., McFadden, L. D., Rockwell, T. K., Shroba, R. R., et al. (1995). Quaternary soils and dust deposition in southern Nevada and California. *Geological Society of America Bulletin*, *107*(9), 1003–1022. https://doi.org/10.1130/0016-7606(1995)107<1003:QSADDI>2.3.CO;2

Reheis, M.C., Budahn, J.R., & Lamothe, P.J. (2002). Geochemical evidence for diversity of dust sources in the southwestern United States. *Geochimica et Cosmochimica Acta, 66,* 1569–1587. doi: 10.1016/S0016-7037(01)00864-X

Reheis, M. C., Budahn, J. R., Lamothe, P. J., & Reynolds, R. L. (2009). Compositions of modern dust and surface sediments in the Desert Southwest, United States. *Journal of Geophysical Research: Earth Surface*, *114*(1), 1–20. https://doi.org/10.1029/2008JF001009

Reheis, M. C., Bright, J., Lund, S. P., Miller, D. M., Skipp, G., & Fleck, R. J. (2012). A half-million-year record of paleoclimate from the Lake Manix Core, Mojave Desert, California. *Palaeogeography, Palaeoclimatology, Palaeoecology, 365*, 11-37.

Reynolds, R. L., Reheis, M., Yount, J., & Lamothe, P. (2006). Composition of aeolian dust in natural traps on isolated surfaces of the central Mojave Desert - Insights to mixing, sources, and nutrient inputs. *Journal of Arid Environments*, *66*(1), 42–61. https://doi.org/10.1016/j.jaridenv.2005.06.031

Rogers, C. L., Cram, C. M., Pease, M. H., & Tischler, M. S. (1977). *Geologic Map of the Yabucoa and Punta Tuna Quadrangles, Puerto Rico* (No. 77-651). US Geological Survey.

Smalley, I. (1995). Making the material: The formation of silt sized primary mineral particles for loess deposits. *Quaternary Science Reviews*, *14*(7–8), 645–651. https://doi.org/10.1016/0277-3791(95)00046-1

Smalley, I. J., & Vita-Finzi, C. (1968). The formation of fine particles in sandy deserts and the nature of "desert' loess. *Journal of Sedimentary Research, 38*(3), 766-774.

Smalley, I. J., & Krinsley, D. H. (1978). Loess deposits associated with deserts. *Catena, 5*(1), 53–66. https://doi.org/10.1016/S0341-8162(78)80006-X.

Smith, B. J., Wright, J. S., & Whalley, W. B. (2002). Sources of non-glacial, loess-size quartz silt and the origins of "desert loess". *Earth-Science Reviews, 59*(1-4), 1-26.

Soreghan, L. S., Soreghan, M. J., & Hamilton, M. A. (2008). Origin and significance of loess in late Paleozoic western Pangaea: A record of tropical cold*? Palaeogeography, Palaeoclimatology, Palaeoecology, 268*(3-4), 234–259. https://doi.org/10.1016/j. palaeo.2008.03.050

Soreghan, G. S., Joo, Y. J., Elwood Madden, M. E., & Van Deventer, S. C. (2016). Silt production as a function of climate and lithology under simulated comminution. *Quaternary International*, *399*, 218–227. https://doi.org/10.1016/j.quaint.2015.05.010

Sun, J. (2002). Provenance of loess material and formation of loess deposits on the Chinese Loess Plateau. *Earth and planetary science letters*, *203*(3-4), 845-859.

Swet, N., Elperin, T., Kok, J. F., Martin, R. L., Yizhaq, H., & Katra, I. (2019). Can active sands generate dust particles by wind-induced processes?. *Earth and Planetary Science Letters, 506,* 371-380.

Taboada, T., & Garcia, C. (1999). Smectite formation produced by weathering in a coarse granite saprolite in Galicia (NW Spain). *Catena*, *35*(2-4), 281-290.

Taylor, S. R., & McLennan, S. M. (1985). *The continental crust: its composition and evolution.* Blackwell Scientific.

Taylor, S. R., & Mclennan, S. M. (1995). The geochemical evolution of the continental crust. *Reviews in Mineralogy and Geochemistry*, *33*(2), 241–265.

Teruggi, M. E. (1957). The nature and origin of Argentine loess. *Journal of Sedimentary Research*, *27*(3), 322-332.

Tsoar, H., & Pye, K. (1987). Dust transport and the question of desert loess formation. *Sedimentology, 34*(1), 139–153. https://doi.org/10.1111/j.1365-3091.1987. tb00566.x.

Turner, S., Hawkesworth, C., Van Calsteren, P., Heath, E., Macdonald, R., & Black, S. (1996). U-series isotopes and destructive plate margin magma genesis in the Lesser Antilles. *Earth and Planetary Science Letters*, *142*(1-2), 191-207.

Wang, C., Ross, G. J., & Rees, H. W. (1981). Characteristics of residual and colluvial soils developed on granite and of the associated pre-Wisconsin landforms in north-central New Brunswick. *Canadian Journal of Earth Sciences*, *18*(3), 487-494.

Wang, H., Mason, J. A., & Balsam, W. L. (2006). The importance of both geological and pedological processes in control of grain size and sedimentation rates in Peoria Loess. *Geoderma*, *136*(1-2), 388-400.

Weigelt, P., Steinbauer, M. J., Cabral, J. S., & Kreft, H. (2016). Late quaternary climate change shapes island biodiversity. *Nature*, *532*(7597), 99–102. https://doi.org/10.1038/nature17443

Wentworth, C. K. (1922). A scale of grade and class terms for clastic sediments. *The journal of geology, 30*(5), 377-392.

White, A. F. (2002). Determining mineral weathering rates based on solid and solute weathering gradients and velocities: Application to biotite weathering in saprolites. *Chemical Geology*, *190*(1–4), 69–89. https://doi.org/10.1016/S0009-2541(02)00111-0

White, A.F., Blum, A.E., Schultz, M.S., Vivit, D.V., Stonestrom, D.A., Larsen, M., Murphy, S.F., and Eberl, D. (1998,). Chemical weathering in a tropical watershed, Luquillo Mountains, Puerto Rico: I. Long-term versus short-term weathering fluxes: *Geochimica et Cosmochimica*, *62*, 209–226. https:// doi .org /10 .1016 /S0016 -7037 (97)00335 -9.

White, A. F., & Buss, H. L. (2014). 7.4-Natural weathering rates of silicate minerals. *Treatise on Geochemistry, Second Edition. Elsevier, Oxford*, 115-155.

Wright, J. (2001). Making loess-sized quartz silt: Data from laboratory simulations and implications for sediment transport pathways and the formation of “desert” loess deposits associated with the Sahara. *Quaternary International*, *76–77*, 7–19. https://doi.org/10.1016/S1040-6182(00)00085-9

Wright, J. S. (2002a). Particle size characteristics and quartz microfracture patterns in I-and S-type granitoid weathering profiles: some preliminary observations from Eastern Australia. *Transactions of the Japanese Geomorphological Union*, *23*, 309-334.

Wright, J. S. (2002b). Granitoid weathering profiles as a source of loessic silt. *Transactions of the Japanese Geomorphological Union*, *23*(5), 769-793.

Wright, J. S. (2007). An overview of the role of weathering in the production of quartz silt. *Sedimentary Geology*, *202*(3), 337–351. https://doi.org/10.1016/j.sedgeo.2007.03.024

Wright, J., & Smith, B. (1993). Fluvial Comminution and the Production of Loess-Sized Quartz Silt: A Simulation Study. *Geografiska Annaler. Series A, Physical Geography*, *75*(1/2), 25–34.

Wright, J., Smith, B., & Whalley, B. (1998). Mechanisms of loess-sized quartz silt production and their relative effectiveness: Laboratory simulations. *Geomorphology*, *23*(1), 15–34. https://doi.org/10.1016/S0169-555X(97)00084-6

Yaalon, D. H., & Ganor, E. (1973). The influence of dust on soils during the Quaternary. *Soil Science*, *116*(3), 146-155.

Zárate, M., & Blasi, A. (1993). Late Pleistocene-Holocene eolian deposits of the southern Buenos Aires Province, Argentina: a preliminary model. *Quaternary International*, *17*, 15-20.

Zhu, Y., Jia, X., & Shao, M. (2018). Loess Thickness Variations Across the Loess Plateau of China. *Surveys in Geophysics*, *39*(4), 715–727. https://doi.org/10.1007/s10712-018-9462-6